Structural Comparison of Monomeric Variants of the Chemokine MIP-1β Having Differing Ability To Bind the Receptor CCR5[†,‡]

Seho Kim, Shu-chuan Jao, Jennifer S. Laurence,[§] and Patricia J. LiWang*

Department of Biochemistry and Biophysics, Texas A&M University, TAMU 2128, College Station, Texas 77843-2128

Received May 23, 2001

ABSTRACT: MIP-1β, a member of the chemokine family of proteins, tightly binds the receptor CCR5 as part of its natural function in the immune response, and in doing so also blocks the ability of many strains of HIV to enter the cell. The single most important MIP-1β residue known to contribute to its interaction with the receptor is Phe13, which when mutated reduces the ability of MIP-1β to bind to CCR5 by more than 1000-fold. To obtain a structural understanding of the dramatic effect of the absence of Phe13 in MIP-1β, we used multidimensional heteronuclear NMR to determine the three-dimensional structure of the MIP-1β F13A variant. We had previously shown that, unlike the wild-type protein which has been shown to be a tight dimer, the F13A mutant is monomeric even at high concentrations [Laurence, J. S., Blanpain, C., Burgner, J. W., Parmentier, M., and LiWang, P. J. (2000) *Biochemistry 39,* 3401−3409], leading to significant changes in the NMR spectra of F13A and the wild-type protein. We have obtained a total of 940 structural restraints for MIP-1β F13A, and have calculated a family of structures having a backbone rmsd from the average of 0.55 Å (residues 12−67). A structural comparison of the F13A mutant with a fully active monomeric variant, P8A, shows that despite some differences in the $^{1}H-^{15}N$ HSQC spectra the two are nearly identical in NOE distance restraints and in backbone conformation. A comparison of F13A with the wild-type protein shows largely the same fold, although differences exist in the N-terminal and loop regions for which the loss of the dimer in F13A can mainly account. A dynamics comparison confirms greater flexibility in F13A than in the wild-type protein in regions of dimer contact in the wild-type protein. In an analysis to determine if the large functional effect resulting from the loss of Phe13 is due to the local side chain change or due to more global structural changes, we conclude that local effects predominate. This suggests that a strategy for designing tight binding anti-CCR5 therapeutics should include a Phe-like component.

Chemokines (chemotactic cytokines) form a family of small immune system proteins that are involved in neutrophil and monocyte activation and chemotaxis. The family is further divided into subfamilies that are named on the basis of the placement of conserved cysteines at the N-terminus of the protein. The two largest subfamilies are the CC (containing two contiguous cysteines) and the CXC (containing an amino acid between the two conserved cysteines) subfamilies. Due to their vital role in immune processes such as inflammation and localization of leukocytes, chemokines not only are necessary for a functional immune system (*1*),- but also have been implicated in a wide variety of disorders ranging from allergic reactions (*2*) to viral-induced heart inflammation (*3*). In addition, a few chemokines, including MIP-1β,[1] the subject of the work presented here, have been shown to have the ability to inhibit infection by HIV (*4*−*6*). This activity arises from the use by HIV of some chemokine receptors as entry portals to the cell. The cell surface receptor CCR5 is a seven-transmembrane G-protein-coupled receptor that normally binds to CC chemokines such as MIP-1β, MIP-1α, and RANTES (*7*, *8*). Many strains of HIV are able to use CCR5 as a coreceptor for entry along with another cell surface protein, CD4 (*4*−*6*), and it is believed that CCR5 facilitates infection by strains of HIV that are crucial for establishing initial infection (*2*). However, when chemokine

[†] Funding was provided by the Robert A. Welch Foundation A1472 and by the National Science Foundation (Grant MCB 9733907).

[‡] The average minimized structure of MIP-1β F13A has been deposited to the Protein Data Bank and can be accessed as 1JE4.

* To whom correspondence should be addressed: Department of Biochemistry and Biophysics, Texas A&M University, TAMU 2128, College Station, TX 77843-2128. E-mail: pliwang@tamu.edu. Telephone: (979) 845-5616. Fax: (979) 845-9274.

[§] Current address: Department of Biological Sciences, Purdue University, 1392 Lilly Hall, West Lafayette, IN 47907-1392.

[1] Abbreviations: CCR, CC chemokine receptor; COSY, correlated spectroscopy; DSS, 2,2-dimethyl-2-silapentane-5-sulfonic acid; HCC, human CC chemokine; HIV, human immunodeficiency virus; HSQC, heteronuclear single-quantum coherence; IC_{50}, median inhibitory concentration; IL-8, interleukin-8; INEPT, insensitive nuclei enhanced by polarization transfer; K_d, dissociation constant; K_i, inhibitory dissociation constant in a competition binding assay; MCP, monocyte chemoattractant protein; MIP, macrophage inflammatory protein; MPIF, myeloid progenitor inhibitory factor; NOE, nuclear Overhauser effect; NOESY, nuclear Overhauser effect spectroscopy; rmsd, root-mean-square deviation; RANTES, regulated on activation of normal T cell expressed and secreted; TOCSY, total correlation spectroscopy; T_1, longitudinal relaxation time; T_2, transverse relaxation time; R_1, longitudinal relaxation rate ($1/T_1$); R_2, transverse relaxation rate ($1/T_2$); τ_m, rotational correlation time; τ_e, effective correlation time for internal motions; S^2, square of the generalized order parameter; S_s^2 and S_f^2, squares of order parameters on slow and fast time scales, respectively; R_{ex}, chemical exchange contribution to R_2; SSE, sum of squared errors; vMIP, viral macrophage inflammatory protein; WT, wild type.

10.1021/bi011065x CCC: $20.00
Published on Web 08/17/2001

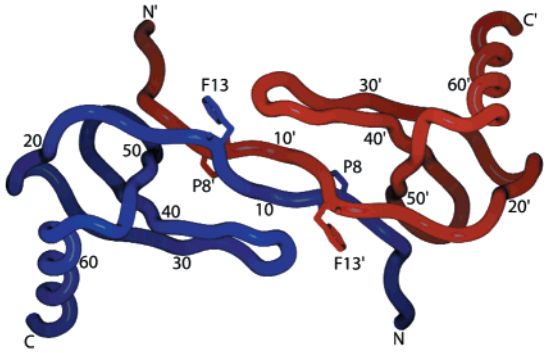

FIGURE 1: NMR solution structure of MIP-1β (*10*). Most of the dimer contacts are in the N-terminal (residues 4−9) and N-loop (residues 13−19) regions. The side chains of residues F13 and P8 are shown to indicate the sites of mutation in this study.

ligands such as MIP-1β are bound to CCR5, HIV infection is blocked, likely via a combination of steric interference and endocytosis of the receptor (*9*).

The structures of many CC chemokines, including MIP-1β (*10*), MIP-1α (*11*), and RANTES (*12*), show a protein dimer with the dimer interface being located along the N-terminus of each subunit (Figure 1 shows the structure of MIP-1β). However, a variant of the CXC chemokine IL-8 was shown to be functional as a monomer (*13*), leading to speculation that despite the chemokine propensity to dimerize, the functional chemokine unit may be the monomer. In CC chemokines, this "active monomer" hypothesis was supported by work on MCP-1 variants (*14*) and by our work on MIP-1β (*15*). In the latter study, two mutants of MIP-1β were shown to be particularly important. First, the P8A variant was shown to be fully monomeric under NMR conditions and yet to be nearly fully functional, in both its binding and activation of CCR5. Second, and perhaps more intriguing, the F13A variant was demonstrated to be a folded monomer but yet to be almost entirely unable to bind the CCR5 receptor, having a K_i of >1 μM, as compared to a K_i of 0.39 nM for the wild-type protein (*15*). The functional importance of the residue at position 13 of MIP-1β was further demonstrated by a series of mutations at this position that showed a requirement for a large aromatic group for the optimal interaction of this chemokine with its receptor. In addition, the importance of this position for function and dimerization has also been demonstrated in other CC chemokines (*14*, *16*−*18*).

Despite the importance of the chemokine monomer and in particular of the monomeric F13A variant which with one point mutant apparently abrogates the CCR5 binding ability of the chemokine, no structure has yet been reported for a monomeric form of any of the three human anti-HIV CC chemokines, namely, MIP-1β, MIP-1α, or RANTES. There are two reasons why it would be especially desirable to have structural information for a monomer of these chemokines. First, the location of their dimer interface at the N-terminus overlaps closely with the functional regions of the protein: some of the first nine residues of these chemokines are believed to be important for activation of CCR5, while the N-loop region (residues 13−19) has been shown to contain several of the amino acids that are important for binding the receptor (*14*−*16*, *19*, *20*). Since each determined structure is a dimer (with similar regions of the protein important both to maintaining dimer structure and to chemokine function), the monomeric form of the protein might show large differences from the known structures, particularly in these key regions. Second, and in support of the possibility of structure differing between the monomer and dimer, the ^{1}H−^{15}N HSQC NMR spectra of the monomeric variants of MIP-1β are quite different from that of the wild-type protein, raising the possibility of a structurally changed environment for many residues (Figure 2).

We have undertaken a structural study of two important monomeric variants of MIP-1β. We report the full NMR structure determination of the F13A mutant of MIP-1β. We also compare the spectra for this mutant to those of the active monomer P8A and compare the structural features of these two variants. Finally, we compare the F13A structure to the known structure of wild-type MIP-1β and analyze the regions of structure that are retained in the monomeric and dimeric forms, and the regions in which the structures deviate. In addition, we address the important question of whether the loss of CCR5 binding ability of the F13A mutant may be

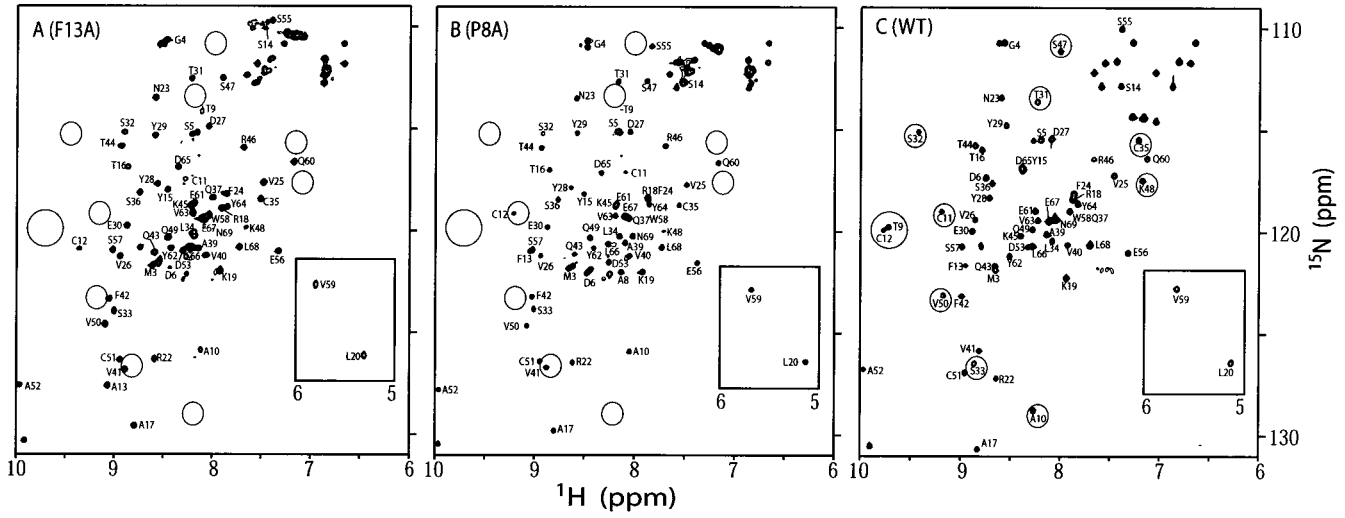

FIGURE 2: Assigned ^{1}H−^{15}N HSQC spectra of MIP-1β F13A (A), P8A (B), and WT (C). Circles are drawn in positions identical to those of the peaks representing the dimeric form to highlight differences in chemical shifts between the monomer and dimer. The peaks found at low ^{1}H values (parts per million) are boxed in each spectrum.

from global structural changes or from local amino acid interactions. A purely local effect due to the presence or absence of F13 would suggest the desirability of a similar moiety in the design of a tight binding anti-CCR5 therapeutic.

MATERIALS AND METHODS

Protein Preparation. Proteins of MIP-1β WT (wild-type), MIP-1β F13A (called simply F13A), and MIP-1β P8A (called simply P8A) were expressed in *Escherichia coli* and purified following previously reported methods (*15*). ^{15}N- and ^{15}N/^{13}C-labeled proteins (1−2 mM) were prepared in 20 mM sodium phosphate buffer (pH 2.5) and 10% D_2O for NMR spectroscopy.

NMR Spectroscopy. All NMR spectra were acquired at 25 °C on Varian INOVA 500 or 600 MHz NMR spectrometers. Chemical shifts were referenced to DSS by the method of Wishart et al. (*21*). For comparison of MIP-1β WT, F13A, and P8A, ^{1}H−^{15}N HSQC (*22*), NOESY-(^{15}N)HSQC (*23*), and *J*-correlated HNHA (*24*) spectra were acquired. Chemical shift assignments of MIP-1β WT were obtained from previous results (*10*). For backbone assignments of P8A, HNCO, HN(CA)CO, HN(CO)CA, HNCA, HA(CACO)NH, HA(CA)NH, and HCACO spectra were acquired (*25*). For backbone assignments of F13A, CBCA(CO)NH (*26*), CBCANH, HBHA(CO)NH, and HBHANH spectra were acquired (*25*). Side chain assignments of F13A were determined using TOCSY-(^{15}N)HSQC (*27*), two three-dimensional HCCH-TOCSY (*28*) experiments with {^{13}C, ^{13}C, ^{1}H} and {^{1}H, ^{13}C, ^{1}H} detection, and HCCH-COSY (*29*). To obtain aromatic side chain assignments of F13A, an aromatic HCCH-TOCSY spectrum and NOEs to β-protons in NOESY-(^{15}N)HSQC and NOESY-(^{13}C)HSQC (*30*) spectra were used. NOE constraints for structure calculation of F13A were obtained from NOESY-(^{15}N)HSQC and NOESY-(^{13}C)-HSQC experiments using a mixing time of 150 ms. $^3J_{HN\alpha}$ coupling constants were calculated from HNHA quantitative *J* correlation experiments (*24*). For stereospecific H$^\beta$ assignments and χ_1 angles, HNHB (*31*), TOCSY-(^{13}C)HSQC with a mixing time of 20 ms, and NOE intensity patterns in NOESY-(^{15}N)HSQC were analyzed. In addition, χ_1 information for valine and threonine was obtained from ^{13}C−{^{15}N} spin-echo difference CT-HSQC and ^{13}C−{^{13}CO} spin-echo difference CT-HSQC spectra (*32*).

Structure Calculations. Interproton distance restraints (1.8−2.7, 1.8−3.3, and 1.8−5.0 Å) were obtained from grouped peak intensities (strong, medium, and weak) of assigned NOE cross-peaks. In these restraints, 0.2 Å was added to the upper bound for each NOE involving H^N and 0.5 Å was added for each NOE involving a methyl group. $^3J_{HN\alpha}$ coupling constants (*24*) were converted to backbone ϕ angle restraints as follows: $-60 \pm 30°$ for $^3J_{HN\alpha} \leq 5.5$ Hz, $-120 \pm 30°$ for $^3J_{HN\alpha} \geq 8.5$ Hz, $-120 \pm 60°$ for 7.0 Hz $\leq {}^3J_{HN\alpha} < 8.5$ Hz, and $-100 \pm 80°$ for 5.5 Hz $< {}^3J_{HN\alpha} < 7.0$ Hz. χ_1 angles that could be determined from the NMR data were constrained to 60°, −60°, or 180° with a 30° error range. With these distance and dihedral angle restraints, structures were calculated using the simulated annealing protocol (*33*, *34*) after first using distance geometry and simulated annealing (*35*) within the program CNS (*36*). To identify possible hydrogen bonds, the calculated structures and NOEs consistent with secondary structural elements were inspected and 10 hydrogen bonds were used as restraints in the later stages of refinement.

Relaxation Measurements and Analysis. ^{15}N T_1 and T_2 relaxation data were acquired by arrays of ^{1}H−^{15}N HSQC with doubly refocused INEPT (*37*). For MIP-1β F13A, the used time arrays were 80, 160, 240, 360, 480, 600, 760, and 920 ms for T_1 and 16, 32, 48, 72, 96, 120, 152, 184, and 216 ms for T_2. For MIP-1β WT, the used time arrays were 20, 60, 120, 250, 360, 520, 760, and 1000 ms for T_1 and 16, 32, 48, 80, 96, 112, 144, and 160 ms for T_2. These arrays were randomized and cycled first in each time increment of the indirect dimension (t_1). The relaxation delay was 3 s for each scan, and 1024 (t_2) × 192 (t_1) complex data points were collected. ^{15}N−{^{1}H} NOEs were acquired by two arrays of ^{1}H−^{15}N HSQC with single refocused INEPT starting from ^{15}N magnetization (*37*). Two arrays were cycled with and without ^{1}H presaturation for 3 s, and two arrayed spectra were collected in the same manner as T_1 and T_2 acquisitions. The total relaxation delay was 6 s, including the presaturation period.

R_1 ($1/T_1$) and R_2 ($1/T_2$) values were obtained from the exponential fit of the data, and NOEs were calculated by the intensity ratio of the two arrayed spectra. To gain physical insight into the motion, the simple isotropic Lipari−Szabo model-free analysis (*38*, *39*) was performed by using the dynamics software Modelfree 4.0 (*40*). First, a local τ_m on each residue was calculated, and then an averaged τ_m was obtained as a best τ_m for the protein using only those residues with an NOE of >0.65. Then, including only local τ_m values within one standard deviation of the average τ_m, we calculated a final average τ_m. Second, with this fixed average τ_m, five different models of the internal motion were used to fit the relaxation data. Model 1 is a standard Lipari−Szabo model, including only S_s^2, the order parameter on a picosecond time scale. Model 2 includes S_s^2 and the addition of a parameter (τ_e) representing an internal correlation time. Model 3 includes both S_s^2 and an exchange term on the millisecond time scale, R_{ex}. Model 4 includes all three parameters (S_s^2, τ_e, and R_{ex}). Model 5 includes S_s^2 and τ_e as well as S_f^2, an order parameter representing motion on a time scale ~1 order of magnitude faster than that for S_s^2 (*40*, *41*). Finally, a best model for each residue was selected by examining SSE (sum of squared errors) of modeling or errors on parameter values. SSE is defined as $(R_1 - R_1')^2/\sigma_{R_1}^2 + (R_2 - R_2')^2/\sigma_{R_2}^2 + (\mathrm{NOE} - \mathrm{NOE}')^2/\sigma_{\mathrm{NOE}}^2$, where R_1', R_2', and NOE′ are back-calculated values of R_1, R_2, and NOE and σ_{R_1}, σ_{R_2}, and σ_{NOE} are experimental uncertainties in R_1, R_2, and NOE, respectively.

RESULTS

Comparison of F13A to P8A. We have previously reported that monomeric variants of MIP-1β have wide-ranging abilities to function on the MIP-1β receptor CCR5, with the F13A mutation showing the greatest loss of CCR5 binding ability, while the P8A mutation results in a nearly fully active monomer (*15*). However, comparison of the ^{1}H−^{15}N HSQC spectra of monomeric P8A and monomeric F13A proteins revealed only minor differences in cross-peaks. To investigate the backbone of each of these mutants, chemical shift assignments, consisting of ^{1}H^N, ^{15}N, ^{1}H$^\alpha$, and ^{13}C$^\alpha$, were completed.

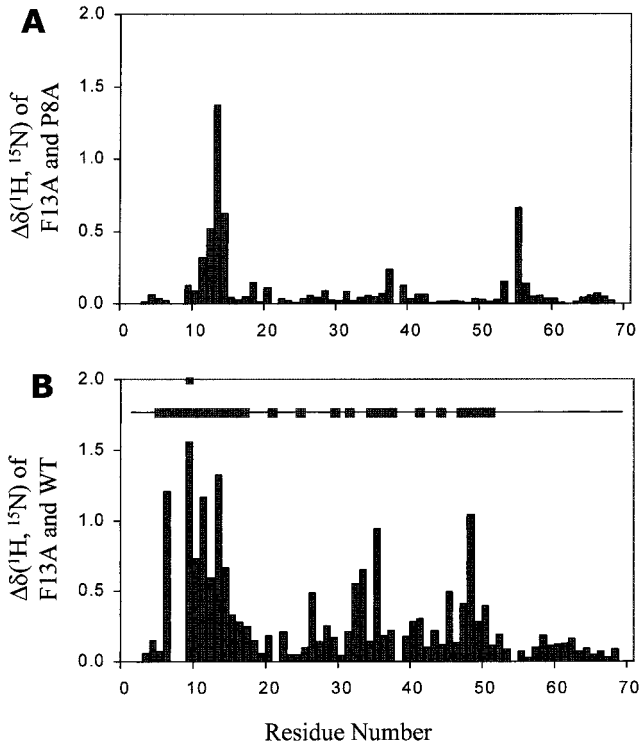

FIGURE 3: Weighted average chemical shift difference, $\Delta\delta$(^{1}H, ^{15}N), in the ^{1}H$-^{15}$N HSQC spectra shown in Figure 2. (A) Difference between MIP-1β F13A and P8A. (B) Difference between MIP-1β F13A and WT. $\Delta\delta$(^{1}H, ^{15}N) is calculated as $|\Delta$ppm of ^{1}H$| + 0.2|\Delta$ppm of ^{15}N$|$, where Δppm is the chemical shift difference (*42*, *43*). Residues that come within 5 Å of the other subunit in the MIP-1β dimer are represented by horizontal bars in panel B.

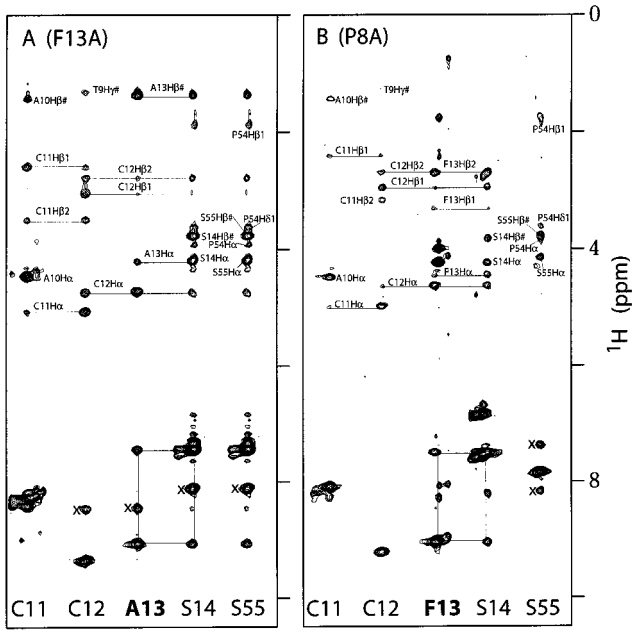

FIGURE 4: NOESY-(^{15}N)HSQC strip plots of MIP-1β F13A (A) and P8A (B). The selected residues in strip plots are those that show significant changes in weighted average chemical shift, $\Delta\delta$-(^{1}H, ^{15}N), between the F13A and P8A variants of MIP-1β as shown in Figure 3A. S14 and S55 of F13A are found on the same strips due to the almost identical chemical shifts of ^{1}H and ^{15}N. Unassigned peaks are marked with an x.

Overall, there is a great deal of similarity in the backbone chemical shifts of F13A and P8A, making it likely that these two variants share a similar overall structure. As shown in panels A and B of Figure 2, the ^{1}H$-^{15}$N HSQC spectrum of F13A is quite similar to that of P8A, but a few variations can be observed between the two proteins. In a comparison of weighted average H^N and ^{15}N chemical shift values (*42*, *43*) for the F13A and P8A variants (Figure 3A), there are two regions where chemical shift differences are most prominent: the residues near position 13 (including position 13 itself, which would obviously have different chemical shifts depending on whether it was an Ala as in the F13A mutant or a Phe in the P8A mutant) and residue 55 which is far in sequence from position 13. However, these chemical shift changes do not confirm local structural differences between the two MIP-1β variants, as it is possible that side chain differences cause the chemical shift changes without alteration of the local backbone conformation.

In light of the several differences in chemical shifts between the two monomeric variants, we decided to further analyze the possible structural difference by acquiring quantitative $^3J_{HNH\alpha}$-correlated HNHA and NOESY-(^{15}N)-HSQC spectra of those two proteins. The HNHA spectrum was used to determine the coupling constant between the H^N and H$^\alpha$ protons ($^3J_{HNH\alpha}$) (*24*) of both the F13A mutant and the P8A mutant. This coupling constant is sensitive to the backbone ϕ angle and so is a good indicator of overall structural similarity between the two variants. We found only small differences in the $^3J_{HNH\alpha}$ values of the two variants in which the maximum difference is ~1.0 Hz (data not shown), indicating no significant difference in the secondary structures for F13A and P8A. A residue by residue analysis of the NOESY-(^{15}N)HSQC spectra of the two variants revealed that the two spectra were nearly identical. Figure 4 shows a portion of those spectra from both the F13A variant and the P8A variant and reveals essentially the same NOE distance contacts despite backbone NH chemical shift differences in the above-mentioned regions in Figure 3A.

In aggregate, our comparison of F13A and P8A in terms of chemical shift, NOESY distance restraints, and $^3J_{HNH\alpha}$ values leads us to conclude that these two structures are essentially identical. Therefore, the dramatic activity loss in the F13A variant as compared to the near-wild-type function of the monomer P8A is largely due to the local effect of the loss of the side chain Phe at position 13. The large chemical shift differences between F13A and P8A are likely not due to conformational change but are simply due to side chain effects, particularly from the presence or absence of the Phe side chain at position 13.

Comparison of Monomer Variants and Wild-Type MIP-1β. In contrast to a comparison between monomers, there are large differences between the ^{1}H$-^{15}$N HSQC spectra of the wild-type MIP-1β and those of monomeric variants such as F13A and P8A (Figure 2). A comparison of weighted average H^N and ^{15}N chemical shifts (*42*, *43*) of F13A and WT (Figure 3B) shows large differences over many residues, especially including the residues at the N-terminus from residues 6−16; residues 32, 33, and 35; residue 45; and residues 47−50. We had previously used a comparison of ^{15}N T_1/T_2 relaxation ratios to determine that the F13A and P8A mutants are monomeric (*15*). To confirm here that the intermolecular contacts in wild-type MIP-1β are clearly lost in the monomeric mutants, we examined NOESY-(^{15}N)-HSQC spectra on the residues involved in the dimerization

(Figure 1). In NOESY-(^{15}N)HSQC strip plots, intermolecular NOEs on the residues found in the dimer interface of MIP-1β WT were clearly missing in both F13A and P8A (data not shown). These missing intermolecular NOEs and previous ultracentrifugation data and ^{15}N relaxation data (*15*) confirmed that single-point mutations such as F13A and P8A abolished dimer formation even at a protein concentration of 1.0−2.0 mM. As the dimer dissociation constant of wild-type MIP-1β is 0.73 μM (albeit under higher-salt conditions) (*15*), the self-binding affinity of each F13A and P8A monomeric mutant has been reduced more than 1000-fold.

To determine whether the large chemical shift differences can be related to structural changes between the monomer and dimer forms of MIP-1β or are due solely to the loss of dimerization in the wild-type protein, we investigated the possibility of a correlation between residues showing large chemical shift changes between F13A and WT and those at the dimer interface. A comparison of the residues having protons in close contact (within 5 Å) with the other polypeptide chain in the dimer structure of wild-type MIP-1β with the residues having chemical shift differences between F13A and WT is shown in Figure 3B. This figure (with an inset showing residues involved in dimer contact) provides a clear rationale for some of the chemical shift differences as a primary effect; in the regions where the F13A mutation has removed MIP-1β dimer contacts, large chemical shift changes result. However, there were also chemical shift differences in some residues (such as residues 25, 32, 33, and 45) that are not directly in the dimer interface, so these chemical shift changes may not be related simply to the loss of the dimer in F13A. Therefore, it is possible that conformational change is occurring both at the dimer interface and outside the dimer region. This suggests that the two monomeric forms (F13A and P8A) might be structurally distinct from WT aside from differences in quaternary structure. Furthermore, the monomeric form of MIP-1β is likely to be more relevant to CCR5 binding than the dimeric form since the receptor−ligand dissociation constant is 3 orders of magnitude lower than the dimer dissociation constant of the protein. Therefore, we determined the structure of the F13A monomeric variant both to obtain an accurate model of monomeric MIP-1β and to clarify whether the monomeric structure of MIP-1β has any distinct variation compared to the wild-type protein.

Structure of MIP-1β F13A. A family of 20 structures was calculated from the distance, dihedral angle, and hydrogen bond restraints listed in Table 1. The intraresidue NOE restraints included only nontrivial NOEs by excluding all geminal NOEs and vicinal NOEs absent of stereospecific assignments. Forty-three ϕ and 26 χ_1 dihedral angles were restrained as described in Materials and Methods. Twenty hydrogen bond restraints were added at the later stages of structural refinement, consisting of two restraints (H^N−O and N−O) per hydrogen bond. A total of 940 restraints were used in the structure calculation, leading to 13.6 restraints per residue. Few restraints could be obtained for the N-terminal residues as would be expected, since monomeric chemokines generally have a disordered N-terminus, and this variant is also lacking the N-terminal dimer interface. From residues 12−67, there were 868 restraints, leading to 15.5 restraints per residue in this region. A summary of short-, medium-, and long-range NOEs per residue is shown in Figure 5A. The N-terminal region (residues 1−10) of the protein has the fewest medium- and long-range NOEs, which is typical of a disordered structure. The region with the next fewest number of NOEs consists of residues 32−37, which comprise a loop that in the wild-type protein is involved in dimer contacts.

Table 1: Structural Statistics for the Ensemble of 20 MIP-1β F13A Structures

	all residues	residues 12−67
no. of distance restraints		
intraresidue ($i - j = 0$)	340	301
sequential ($\|i - j\| = 1$)	223	207
medium-range ($\|i - j\| \leq 4$)	103	97
long-range ($\|i - j\| > 4$)	185	179
total	851	784
no. of dihedral angle restraints		
ϕ	43	38
χ_1	26	26
no. of hydrogen bonds (H^N−O and N−O)	20	20
no. of total restraints	940	868
no. of total restraints per residue	13.6	15.5
NOE violations		
>0.05 Å	1.4 ± 1.2	
>0.1 Å	2.2 ± 1.6	
>0.2 Å	1.8 ± 1.5	
>0.3 Å	0.0 ± 0.0	
dihedral violations		
>0.5°	0.0 ± 0.0	
CNS energies (kcal/mol)		
NOE	1.08 ± 1.45	
dihedral	0.01 ± 0.00	
bond	0.87 ± 0.20	
angle	23.25 ± 0.42	
improper	0.74 ± 0.04	
van der Waals	5.42 ± 0.51	
total	31.37 ± 2.08	
rmsd from experimental restraints		
NOE (Å)	0.0031 ± 0.0027	
dihedral angles (deg)	0.0483 ± 0.0073	
rmsd from ideal geometry		
bonds (Å)	0.0009 ± 0.0001	
angles (deg)	0.2813 ± 0.0025	
impropers (deg)	0.0928 ± 0.0023	
Ramachadran analysis (%)		
most favored regions	68.4 ± 4.6	
additional allowed regions	30.6 ± 4.9	
generously allowed regions	1.0 ± 1.2	
disallowed regions	0.0 ± 0.0	
atomic rmsd from mean structure (Å)		
backbone (residues 12−67)	0.55 ± 0.29	
side chain (residues 12−67)	1.00 ± 0.44	
backbone (residues 12−31 and 38−67)	0.47 ± 0.18	
side chain (residues 12−31 and 38−67)	0.93 ± 0.41	

In the ensemble of 20 calculated structures (Figure 6A), there were no NOE violations greater than 0.3 Å and no dihedral angle violations greater than 0.5°. The backbone (N, C^α, and C) rmsd from the average structure after superimposition with well-defined secondary structures is shown by residue in Figure 5B, revealing the highest uncertainty in the N-terminus of the protein which is correlated with fewer NOEs as in Figure 5A. This would be particularly expected for a monomeric variant of MIP-1β, in which the N-terminal region has lost tight dimer contacts found in the wild-type protein. Other regions of higher-than-average deviation from the mean structure include the loop after the first β-strand, and the very C-terminal amino acids of the protein. When the residues that have a relatively high rmsd in the F13A structure (Figure 5B) are compared to the residues found in the dimer interface of MIP-1β WT, the

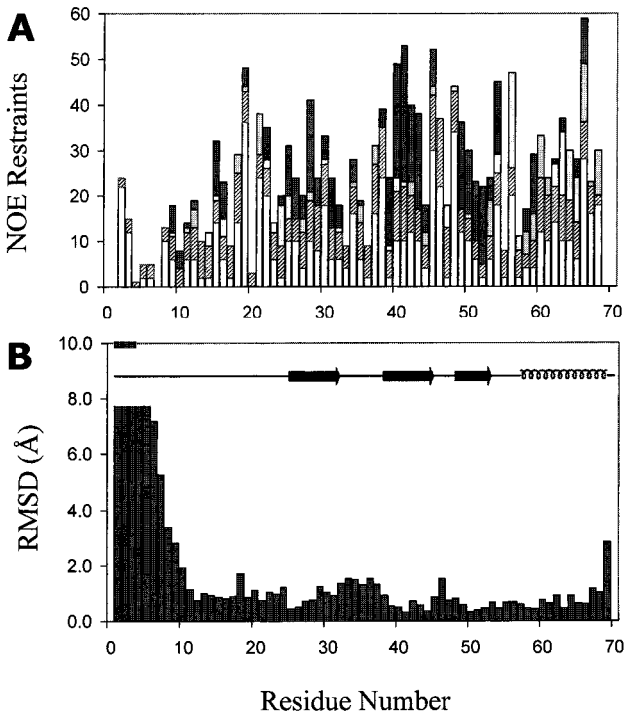

FIGURE 5: NOE restraints (A) and backbone rmsd (B) per residue for the F13A variant of MIP-1β. In panel A, the number of intraresidue (blank), sequential (striped), medium-range (dotted), and long-range (dark gray) NOEs are summarized by residue. In panel B, the rmsd of 20 F13A structures from the average structure is plotted by residue.

poorly defined structural regions in F13A were near the dimer interface except at the C-terminus. As noted in Table 1, the average rmsd from the mean structure for residues 12−67 is 0.55 Å for backbone atoms and 1.00 Å for side chain heavy atoms. When a flexible loop of residues 32−37 is not counted, the rmsd is reduced to 0.47 Å for backbone atoms and 0.93 Å for side chain atoms. If only 27 well-ordered residues (residues 25−29, 40−44, 48−54, and 56−65) are counted in the rmsd calculation, the backbone rmsd is further reduced to 0.38 Å, a level of deviation from the average that is to be expected from a well-defined structure.

The structure of MIP-1β F13A (Figure 6B) shows a clear chemokine fold, consisting of a largely unstructured N-terminus (residues 1−10), followed by a long strand/loop (11−20), leading into a helical turn, and then a three-stranded antiparallel β-sheet (residues 25−31, 38−44, and 48−52). Finally, there is a C-terminal α-helix of residues 57−68. In the antiparallel β-sheet fold, several hydrophobic side chain contacts are found from V25 and Y28 in the first sheet, V40, V41, and F42 in the second sheet, and V50, C51, and A52 in the third sheet. In the C-terminal helix, V63 forms a hydrophobic contact with F42 as does W58 with A52. This hydrophobic core around F42 in the F13A variant is very similar to that of wild-type MIP-1β and indicates that the core structure is not disrupted by the loss of dimerization. As with all members of the CC chemokine family, there are two disulfide bonds that lend stability to the protein. In the F13A variant, the stereochemical orientation of the two disulfide bonds appears to be poorly defined, with the ensemble of structures showing a mixture of both a left-handed spiral and a right-handed hook (*44*). Among all six prolines in the protein, NOE data indicating the trans conformation were confirmed for three proline residues at positions 21, 38, and 54, but the NOE data were insufficient to suggest an orientation for the prolines in the N-terminal region at positions 2, 7, and 8. Each structure in the family of calculated structures showed all trans prolines. For the family of structures, 99% of the backbone dihedral angles were in the "most favored" or "additional allowed" regions of the Ramachandran plot as determined by the program PROCHECK (*45*).

Comparison of F13A Structure and Dynamics to Those of Wild-Type MIP-1β. As noted, there are many large chemical shift differences between F13A and the wild-type MIP-1β, potentially indicating significant differences in

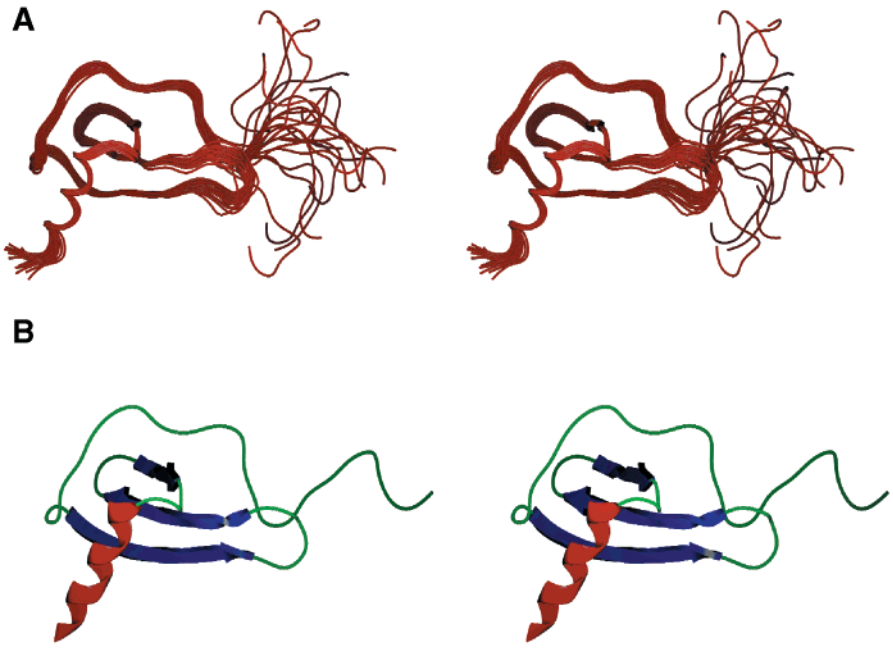

FIGURE 6: Stereoviews of the ensemble (A) and average (B) minimized structures of F13A MIP-1β. In panel A, a family of 20 structures were superimposed using only well-ordered structural regions. In panel B, a ribbon diagram of the average structure shows secondary structures.

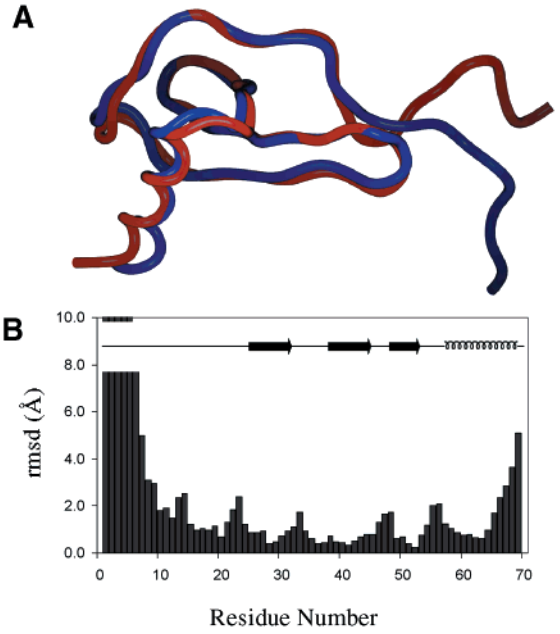

FIGURE 7: Superimposition (A) and backbone rmsd (B) between MIP-1β F13A (red) and WT (blue). NMR average structures of F13A and WT were superimposed using well-ordered structural regions. All secondary structures superimpose quite well, but N- and C-terminal and loop regions do not. The secondary structural elements in MIP-1β are indicated by the inserted bar diagram in panel B.

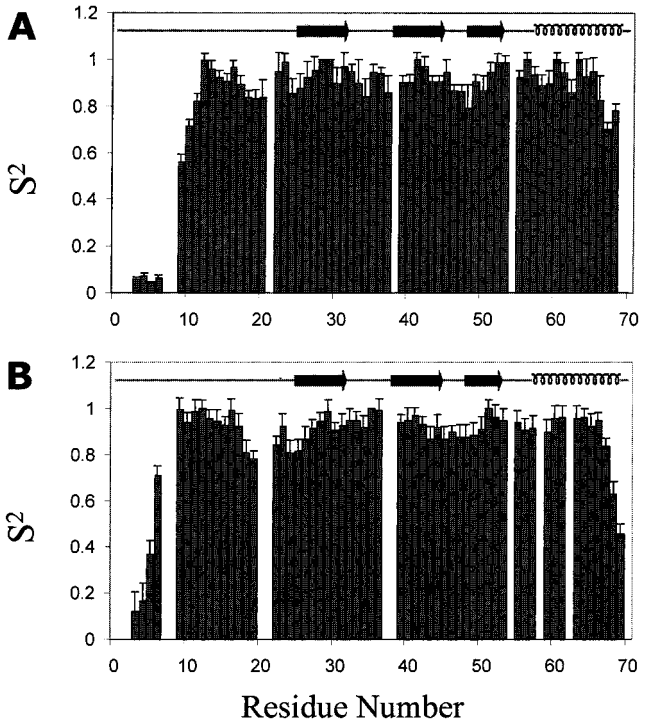

FIGURE 8: Dynamics order parameters (S^2) of MIP-1β F13A (A) and wild-type MIP-1β (B). $S^2 = S_s^2 S_f^2$. S_s^2 and S_f^2 are reported in the Supporting Information, and relaxation data for F13A and WT and parameter values of model-free analyses are also reported. However, the need for order parameters on two time scales is limited, as S_f^2 is 1.0 in all residues except a few N- and C-terminal residues of MIP-1β WT.

structure. A direct comparison of the structure of F13A and the wild-type MIP-1β (*10*) was carried out by overlaying the two structures, first using only well-defined structural regions. The superimposed structures in Figure 7A show that the monomeric F13A structure and a monomeric unit of dimeric wild-type structure are very similar to each other. The loss of dimerization in the F13A variant apparently does not affect the core structure found in the wild-type dimer structure. When the entire structures are compared, the largest deviations are in the N-terminus (residues 1−15, including the F13 mutation), every loop region (residues 22−24, 32−35, 45−48, and 53−56), and the C-terminus. The rmsd of the minimized average F13A structure from the average wild-type monomeric unit is plotted in Figure 7B. As indicated in Figure 7B, major regions with large rmsd values are also at the dimer interface (the N-terminus, 30's loop, and 40's loop). Therefore, the structural deviation between F13A and WT appears to be the result of the loss of dimerization.

The poorly defined structural regions in F13A (Figure 5B) are also a part of the residues that have relatively large rmsd in comparison with the wild-type MIP-1β structure (Figure 7B). This suggests again that the loss of dimerization causes poorly defined structure at the dimer interface and increases the flexibility in the N-terminus and loop regions. Since ^{15}N relaxation parameters (T_1, T_2, and NOE) can be interpreted to distinguish between ordered and flexible backbone conformations, those NMR parameters of F13A and WT were acquired and relevant dynamics parameters were derived by following the model-free approach of Lipari and Szabo (*38*, *39*). In the Supporting Information, the selected model and parameter values of each model are reported residue by residue and the experimentally determined values of T_1, T_2, and NOE and the calculated values from the model are also plotted.

The best τ_m values are 5.52 ns for F13A and 8.07 ns for WT, which agree with the molecular sizes of the monomer and dimer, respectively. By examining five different models of internal motions (for more information, see the Supporting Information), we obtained the best values of the S^2 ($=S_s^2 S_f^2$) order parameter. All S^2 values were actually equal to S_s^2 (not requiring the additional S_f^2 term) except at a few N- and C-terminal residues of WT where S_f^2 parameter values were less than 1.0. S^2 values of MIP-1β and the F13A variant are plotted as a function of residue in Figure 8 to distinguish differences in the motional rigidity of backbone amides. Both proteins were similar in that the first four N-terminal residues and the last three C-terminal residues were quite flexible and the middle regions in sequence indicated restricted motions. In general, the S^2 values of the F13A variant were smaller and more variable than that of the wild-type protein, indicating larger-amplitude fast internal motion for the F13A variant. The greater mobility in the N-terminus of F13A extends up to residue 10; parts of the 30's and 40's loops also show S^2 values slightly smaller than that of the wild-type protein. Another interesting finding is that the extended N-loop near residue 20 and also in the 40's loop in both F13A and the wild-type protein clearly show more flexibility than the other nonterminus regions of either protein. The regions of F13A having low order parameters are closely related to those residues having a large rmsd from the average structure and are also related to the regions of large deviation in the superimposition between F13A and the wild-type protein. Again, this supports our conclusion that the loss of dimerization results in poorly defined structure and increased conformational flexibility in the regions of the protein that

participate in dimerization, particularly the N-terminus and loop regions in F13A.

DISCUSSION

Analysis of the Region around F13. The region of greatest interest to us is that around the F13A mutation. All experimental evidence for CC chemokines points to this position being the most important mediator of chemokine receptor binding (*14*−*16*, *46*), and it is generally accepted that this N-loop region (residues 13−19) is a critical region used by CC chemokines to interact with their receptor (*16*, *20*), although we and others have shown that some distal residues are also involved in chemokine receptor binding (*17*, *18*, *47*). The loss of F13 virtually abrogates the ability of MIP-1β to bind to CCR5, leading to two alternative hypotheses regarding the rationale for the unique importance of Phe at position 13. First, perhaps the effect is a local one, such that direct interaction by the receptor with F13 provides a large part of the interaction energy for the tight binding by MIP-1β to CCR5 (wild-type $K_i = 0.39 \pm 0.12$ nM compared to $K_i > 1000$ nM for F13A) (*15*). Second, the effect may be more global in nature, such that the loss of Phe at position 13 alters the structure of the chemokine to disrupt further-afield contacts in addition to the loss of direct interaction between F13 and the receptor. We find for residues near F13 that the backbone is not disturbed from the active P8A monomeric variant based on both distance [NOESY-(^{15}N)HSQC] and backbone dihedral angle ($^3J_{HNH\alpha}$) data. Therefore, it appears that the side chain difference alone at position 13, rather than any appreciable structural change, is responsible for the 1000-fold loss in the ability of F13A to bind the receptor CCR5. This suggests that the contribution of Phe13 to receptor binding is ~4 kcal/mol.

As mentioned, NMR evidence indicated the possibility of conformational differences between monomeric variants and wild-type MIP-1β, and the family of F13A structures we report have shown minor structural differences with respect to the wild-type protein, especially in the N-terminal and loop regions. However, when comparing the active monomer P8A with the binding-impaired monomer F13A via a careful analysis of distance restraints, chemical shift, and backbone ϕ angles, we show that the structures of P8A and F13A are very similar to each other. Therefore, it appears that the full F13A NMR structure presented here is also an accurate model for the functionally active P8A structure, and so the minor conformational changes between the monomeric variants and the dimeric wild-type protein are likely not important to the functional activity. Therefore, the well-defined N-terminal and N-loop regions in wild-type MIP-1β are likely a consequence of the presence of the tight dimer, but the structural restriction in these regions likely does not play a key role in biological activity.

Structure and Dynamics of the F13A Mutant. Our NMR results show that the loss of dimerization by F13A or P8A mutations is a key factor generating NMR chemical shift, structure, and dynamics differences between these monomers and the wild-type protein. Therefore, although large NMR spectral differences between MIP-1β monomeric mutants and the wild-type protein were observed, most of the well-defined regions of structure, including α-helix and β-sheets in F13A, could be superimposed on the structure of the wild-type protein with little deviation. The effect of the loss of dimerization on the structure was not as severe as might be expected from the large chemical shift changes, and it is therefore likely that a monomeric unit of the determined structure of the wild-type protein (*10*) remains an accurate description of the monomeric molecular form. The poorly determined regions in the N-terminus and loops in the F13A structure (showing a large rmsd from the average structure) indicate the possibility of increased conformational flexibility compared to WT. This hypothesis was supported by ^{15}N relaxation data and a full dynamics analysis, where decreased order parameters were observed for dimer interface regions, including the N-terminus and 30's loop. The best fit values of the S^2 order parameter were able to describe the backbone flexibility of the F13A protein itself and its difference from the wild type without assuming different anisotropic motions for monomer and dimer proteins.

The overall structural quality of the F13A mutant is likely influenced by the increased flexibility caused by the loss of dimer contacts. As shown in Figure 5B, the well-defined secondary structural regions have rmsd values within 0.4 Å of the average structure for the family, while the N-terminal and loop regions, including the extended N-loop, have larger rmsds. All of these regions consist of residues at or near the dimer interface. S^2 values also showed a less ordered backbone conformation in the F13A variant than in the wild-type protein. We have worked with more than 10 monomeric variants of MIP-1β (refs *15*, *47*, and *48*, and unpublished results) and in general have found monomeric variants of MIP-1β to have lower spectral quality (possibly indicative of lower stability) and, in cases where NOESY spectra were acquired, fewer cumulative distance restraints. This smaller number of distance restraints is generally consistent with less precision in the family of structures.

Comparison of F13A to Naturally Occurring Chemokine Monomers. While most chemokines are dimers under conditions required to determine their structure, several chemokines have been shown to be monomeric under at least some high-concentration conditions. The structures of several of these types of chemokines have been determined, including HCC-2 (*49*), MCP-3, I-309 (*50*), eotaxin (*51*), eotaxin-2 (*43*), and MPIF-1 (*52*). These proteins do not bind the CCR5 receptor, but all show the typical chemokine fold. Each of these NMR structures exhibits a relatively large rmsd in the N-terminus, the loop between the first and second β-sheets, and the C-terminus, similar to that observed by us herein for the F13A variant of MIP-1β. The less ordered characteristics in these regions may therefore be a typical dynamic property of monomeric chemokines. This motional disorder has led to similar atomic resolutions among the NMR structures of these naturally occurring monomeric CC chemokine proteins; when the disordered N- and C-terminal regions are excluded, the backbone atomic resolutions of these proteins are the same as for the F13A variant of MIP-1β, ranging from 0.4 to 0.6 Å (*43*, *49*−*52*).

We have previously reported the dynamics (*53*) and structural (*54*) study of vMIP-II, a virally derived chemokine that is able to bind the HIV coreceptor CCR5 tightly; vMIP-II binds to CCR5 with an IC_{50} of 6.2 nM (*55*). We have shown that under many solution conditions vMIP-II remains monomeric (*53*, *54*), although others have crystallized this protein in the dimer form (*56*). Since the present F13A

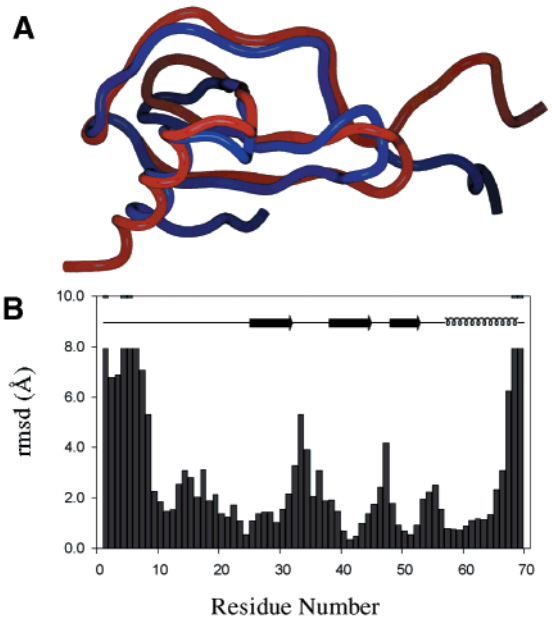

FIGURE 9: Superimposition (A) and backbone rmsd (B) between MIP-1β F13A (red) and vMIP-II. (blue). All secondary structural elements are superimposed well except N- and C-terminal and loop regions. The secondary structural elements in MIP-1β are indicated by the inserted bar diagram in panel B.

structure is very similar to wild-type MIP-1β, the previously reported comparison of a monomeric subunit of MIP-1β structure with the solution structure of vMIP-II (*54*) is valid. However, as seen in Figure 9, despite the fact that the structures of MIP-1β and vMIP-II show almost perfect superposition in regions of secondary structure, these proteins have large differences in the backbone conformation of every loop in addition to the N- and C-terminus. The dynamics data for vMIP-II showed flexibility in the 30's loop between the first and second β-sheets as well as the disorder in the N- and C-termini, but did not show as much flexibility in the 40's loop between the second and third β-sheets and the 50's loop between the third β-sheet and the helix. This may suggest that loop conformations are not important to the receptor binding or that these residues are actually flexible in the slow exchange time scale without obvious chemical shift differences. To determine whether loop flexibility and slow time scale motion is important to binding CCR5, it would be helpful to have a larger set of determined structures and dynamics data for monomeric chemokines that are able to bind CCR5.

Comparison to a Designed IL-8 Monomer. Aside from the structure of MIP-1β variant F13A presented here, only one other structure has been reported of a designed monomeric form of a tight chemokine dimer. The CXC chemokine IL-8 has a dimer K_d of 10 μM (*57*), although this protein is from a different chemokine subfamily and has a completely different dimer interface. The dimer interface of IL-8 is centered on the first β-sheet, with additional interactions from the 30's loop and the C-terminal helix (*58*). The monomeric form of IL-8 was engineered by placement of a chemically modified L25 in the first β-sheet to disallow the H-bonding required for the dimer interaction (*13*). The structure of this monomeric IL-8 showed that the C-terminal helix of residues 67−72 was no longer ordered and the 30's loop was slightly disordered or distorted, but that the first β-sheet was still well-ordered despite the loss of the dimer (*59*). Therefore, like in the MIP-1β F13A variant, the loss of dimerization in IL-8 also resulted in poorly ordered structures in some dimer interface regions of this protein (although due to the different dimer interface, these regions are not identical to the regions that lose order upon loss of the CC chemokine dimer). The retention of structure despite the loss of dimerization in the first β-sheet of IL-8 where the chemical modification resides is likely due to the remaining contacts with other secondary structures, such as the interactions of this β-strand with the adjoining β-strand which form part of the canonical chemokine β-sheet.

CONCLUSION

As it is likely that chemokines bind their receptors as monomers, we have investigated several aspects of both the structure and dynamics of the chemokine MIP-1β and its monomeric variants. Structures of the active (P8A) and inactive (F13A) monomeric variants of MIP-1β were compared by comparing their NMR spectra. In NOESY-(^{15}N)-HSQC and $^{3}J_{HNH\alpha}$-correlated HNHA spectra, the two monomeric variants were almost identical. Therefore, the activity difference between these proteins can be explained by the local side chain effect of an aromatic group at position 13, suggesting that this single side chain contributes 4 kcal/mol in interaction energy between MIP-1β and CCR5. Despite large chemical shift differences between the monomeric variant and the dimeric wild-type protein, the monomeric F13A structure could be superimposed on the wild-type structure except in the N- and C-terminal regions and in loops that are part of the wild-type dimer interface. We conclude that the loss of dimerization results in less ordered structures and increased flexibility in the dimer contact regions without affecting the core structure.

ACKNOWLEDGMENT

The NMR instrumentation in the Biomolecular NMR Laboratory at Texas A&M University was supported by a grant from the National Science Foundation (DBI-9970232) and the Texas A&M University System.

SUPPORTING INFORMATION AVAILABLE

^{15}N R_1, R_2, and NOE NMR relaxation data of MIP-1β F13A and WT and dynamics parameter values (τ_m, τ_e, S_s^2, S_f^2, and R_{ex}) of model-free analyses are available free of charge via the Internet at http://pubs.acs.org.

REFERENCES

1. Baggiolini, M., Dewald, B., and Moser, B. (1997) *Annu. Rev. Immunol. 15*, 675−705.
2. Gerard, C., and Rollins, B. J. (2001) *Nat. Immunol. 2*, 108−115.
3. Cook, D. N., Beck, M. A., Coffman, T. M., Kirby, S. L., Sheridan, J. F., Pragnell, I. B., and Smithies, O. (1995) *Science 269*, 1583−1585.
4. Alkhatib, G., Combadiere, C., Broder, C. C., Feng, Y., Kennedy, P. E., Murphy, P. M., and Berger, E. A. (1996) *Science 272*, 1955−1958.
5. Deng, H., Liu, R., Ellmeier, W., Choe, S., Unutmaz, D., Burkhart, M., Di Marzio, P., Marmon, S., Sutton, R. E., Hill, C. M., Davis, C. B., Peiper, S. C., Schall, T. J., Littman, D. R., and Landau, N. R. (1996) *Nature 381*, 661−666.

6. Dragic, T., Litwin, V., Allaway, G. P., Martin, S. R., Huang, Y., Nagashima, K. A., Cayanan, C., Maddon, P. J., Koup, R. A., Moore, J. P., and Paxton, W. A. (1996) *Nature 381*, 667−673.
7. Combadiere, C., Ahuja, S. K., Tiffany, H. L., and Murphy, P. M. (1996) *J. Leukocyte Biol. 60*, 147−152.
8. Samson, M., Labbe, O., Mollereau, C., Vassart, G., and Parmentier, M. (1996) *J. Biol. Chem. 35*, 3362−3367.
9. Mack, M., Luckow, B., Nelson, P. J., Cihak, J., Simmons, G., Clapham, P. R., Signoret, N., Marsh, M., Stangassinger, M., Borlat, F., Wells, T. N., Schlondorff, D., and Proudfoot, A. E. (1998) *J. Exp. Med. 187*, 1215−1224.
10. Lodi, P. J., Garrett, D. S., Kuszewski, J., Tsang, M. L.-S., Weatherbee, J. A., Leonard, W. J., Gronenborn, A. M., and Clore, G. M. (1994) *Science 263*, 1762−1767.
11. Czaplewski, L. G., McKeating, J., Craven, C. J., Higgins, L. D., Appay, V., Brown, A., Dudgeon, T., Howard, L. A., Meyers, T., Owen, J., Palan, S. R., Tan, P., Wilson, G., Woods, N. R., Heyworth, C. M., Lord, B. I., Brotherton, D., Christison, R., Craig, S., Cribbes, S., Edwards, R. M., Evans, S. J., Gilbert, R., Morgan, P., Randle, E., Schofield, N., Varley, P. G., Fisher, J., Waltho, J. P., and Hunter, M. G. (1999) *J. Biol. Chem. 274*, 16077−16084.
12. Skelton, N. J., Aspiras, F., Ogez, J., and Schall, T. J. (1995) *Biochemistry 34*, 5329−5342.
13. Rajarathnam, K., Sykes, B. D., Kay, C. M., Dewald, B., Geiser, T., Baggiolini, M., and Clark-Lewis, I. (1994) *Science 264*, 90−92.
14. Paavola, C. D., Hemmerich, S., Grunberger, D., Polsky, I., Bloom, A., Freedman, R., Mulkins, M., Bhakta, S., McCarley, D., Wiesent, L., Wong, B., Jarnagin, K., and Handel, T. M. (1998) *J. Biol. Chem. 273*, 33157−33165.
15. Laurence, J. S., Blanpain, C., Burgner, J. W., Parmentier, M., and LiWang, P. J. (2000) *Biochemistry 39*, 3401−3409.
16. Pakianathan, D. R., Kuta, E. G., Artis, D. R., Skelton, N. J., and Hebert, C. A. (1997) *Biochemistry 36*, 9642−9648.
17. Hemmerich, S., Paavola, C., Bloom, A., Bhakta, S., Freedman, R., Grunberger, D., Krstenansky, J., Lee, S., McCarley, D., Mulkins, M., Wong, B., Pease, J., Mizoue, L., Mirzadegan, T., Polsky, I., Thompson, K., Handel, T. M., and Jarnagin, K. (1999) *Biochemistry 38*, 13013−13025.
18. Ye, J., Kohli, L. L., and Stone, M. J. (2000) *J. Biol. Chem. 275*, 27250−27257.
19. Clark-Lewis, I., Kim, K.-S., Rajarathnam, K., Gong, J.-H., Dewald, B., Moser, B., Baggiolini, M., and Sykes, B. D. (1995) *J. Leukocyte Biol. 57*, 703−711.
20. Wells, T. N. C., Power, C. A., Lusti-Narasimhan, M., Hoogewerf, A. J., Cooke, R. M., Chung, C., Peitsch, M. C., and Proudfoot, A. E. I. (1996) *J. Leukocyte Biol. 59*, 53−60.
21. Wishart, D. S., Bigam, C. G., Yao, J., Abildgaard, F., Dyson, H. J., Oldfield, E., Markley, J. L., and Sykes, B. D. (1995) *J. Biomol. NMR 6*, 135−140.
22. Bax, A., Ikura, M., Kay, L. E., Torchia, D. A., and Tschudin, R. (1990) *J. Magn. Reson. 86*, 304−318.
23. Zuiderweg, E. R. P., and Fesik, S. W. (1989) *Biochemistry 28*, 2387−2391.
24. Vuister, G. W., and Bax, A. (1993) *J. Am. Chem. Soc. 115*, 7772−7777.
25. Cavanagh, J., Fairbrother, W. J., Palmer, A. G., III, and Skelton, N. J. (1996) in *Protein NMR Spectroscopy*, pp 410−531, Academic Press, San Diego.
26. Grzesiek, S., and Bax, A. (1992) *J. Am. Chem. Soc. 114*, 6291−6293.
27. Cavanagh, J., and Rance, M. (1992) *J. Magn. Reson. 96*, 670−678.
28. Bax, A., Clore, G. M., and Gronenborn, A. M. (1990) *J. Magn. Reson. 88*, 425−431.
29. Ikura, M., Kay, L. E., and Bax, A. (1991) *J. Biomol. NMR 1*, 299−304.
30. Ikura, M., Kay, L. E., Tschudin, R., and Bax, A. (1990) *J. Magn. Reson. 86*, 204−209.
31. Archer, S. J., Ikura, M., Torchia, D. A., and Bax, A. (1991) *J. Magn. Reson. 95*, 636−641.
32. Bax, A., Vuister, G. W., Grzesiek, S., Delaglio, F., Wang, A. C., Tschudin, R., and Zhu, G. (1994) *Methods Enzymol. 239*, 79−105.
33. Nilges, M., Clore, G. M., and Gronenborn, A. M. (1988) *FEBS Lett. 239*, 129−136.
34. Stein, E. G., Rice, L. M., and Brunger, A. T. (1997) *J. Magn. Reson. B124*, 154−164.
35. Nilges, M., Clore, G. M., and Gronenborn, A. M. (1988) *FEBS Lett. 239*, 317−324.
36. Brunger, A. T., Adams, P. D., Clore, G. M., DeLano, W. L., Gros, P., Grosse-Kunstleve, R. W., Jiang, J.-S., Kuszewski, J., Nilges, N., Pannu, N. S., Read, R. J., Rice, L. M., Simonson, T., and Warren, G. L. (1998) *Acta Crystallogr. D54*, 905−921.
37. Barbato, G., Ikura, M., Kay, L. E., Pastor, R. W., and Bax, A. (1992) *Biochemistry 31*, 5269−5278.
38. Lipari, G., and Szabo, A. (1982) *J. Am. Chem. Soc. 104*, 4546−4559.
39. Lipari, G., and Szabo, A. (1982) *J. Am. Chem. Soc. 104*, 4559−4570.
40. Mandel, A. M., Akke, M., and Palmer, A. G., III (1995) *J. Mol. Biol. 246*, 144−163.
41. Clore, G. M., Driscoll, P. C., Wingfield, P. T., and Gronenborn, A. M. (1990) *Biochemistry 29*, 7387−7401.
42. Shuker, S. B., Hajduk, P. J., Meadows, R. P., and Fesik, S. W. (1996) *Science 274*, 1531−1534.
43. Mayer, K. L., and Stone, M. J. (2000) *Biochemistry 39*, 8382−8395.
44. Richardson, J. S. (1981) *Adv. Protein Chem. 34*, 167−339.
45. Laskowski, R. A., MacArthur, M. W., Moss, D. S., and Thornton, J. M. (1993) *J. Appl. Crystallogr. 26*, 283−291.
46. Mayer, M. R., and Stone, M. J. (2001) *J. Biol. Chem. 276*, 13911−13916.
47. Laurence, J. S., Blanpain, C., De Leener, A., Parmentier, M., and LiWang, P. J. (2001) *Biochemistry 40*, 4990−4999.
48. Laurence, J. S., LiWang, A. C., and LiWang, P. J. (1998) *Biochemistry 37*, 9346−9354.
49. Sticht, H., Escher, S. E., Schweimer, K., Forssmann, W. G., Rosch, P., and Adermann, K. (1999) *Biochemistry 38*, 5995−6002.
50. Keizer, D. W., Crump, M. P., Lee, T. W., Slupsky, C. M., Clark-Lewis, I., and Sykes, B. D. (2000) *Biochemistry 39*, 6053−6059.
51. Crump, M. P., Rajarathnam, K., Kim, K., Clark-Lewis, I., and Sykes, B. D. (1998) *J. Biol. Chem. 273*, 22471−22479.
52. Rajarathnam, K., Li, Y., Rohrer, T., and Gentz, R. (2001) *J. Biol. Chem. 276*, 4909−4916.
53. LiWang, A. C., Cao, J. J., Zheng, H., Lu, Z., Peiper, S. C., and LiWang, P. J. (1999) *Biochemistry 38*, 442−453.
54. LiWang, A. C., Wang, Z.-x., Sun, Y., Peiper, S. C., and LiWang, P. J. (1999) *Protein Sci. 8*, 2270−2279.
55. Kledal, T. N., Rosenkilde, M. M., Coulin, F., Simmons, G., Johnsen, A. H., Alouani, S., Power, C. A., Luttichau, H. R., Gerstoft, J., Clapham, P. R., Clark-Lewis, I., Wells, T. N. C., and Schwartz, T. W. (1997) *Science 277*, 1656−1659.
56. Fernandez, E. J., Wilken, J., Thompson, D. A., Peiper, S. C., and Lolis, E. (2000) *Biochemistry 39*, 12837−12844.
57. Lowman, H. B., Fairbrother, W. J., Slagle, P. H., Liu, J., Shire, S., and Hebert, C. A. (1997) *Protein Sci. 6*, 598−608.
58. Clore, G. M., Appella, E., Yamada, M., Matsushima, K., and Gronenborn, A. M. (1990) *Biochemistry 29*, 1689−1696.
59. Rajarathnam, K., Clark-Lewis, I., and Sykes, B. D. (1995) *Biochemistry 34*, 12983−12990.

BI011065X